JOURNAL OF SOLID STATE CHEMISTRY 9, 176–186 (1974)

Studies of the System $TaS_{2-x}Se_x$*

J. F. REVELLI, JR.† AND W. A. PHILLIPS

Department of Applied Physics, Stanford University, Stanford, California 94305

Received February 1, 1973

Single crystal and powder samples of the system $TaS_{2-x}Se_x$ have been prepared and studied. The range of solubility was found to extend from $x = 0$ to $x = 2.0$. X-Ray analysis has shown that mixed anion samples exhibit a series of hexagonal layered polymorphs similar to those found in TaS_2 and $TaSe_2$, with the a and c lattice parameters increasing monotonically from TaS_2 to $TaSe_2$. Electrical transport properties were measured on single crystals and found to be similar to the end compositions. Organic molecules such as pyridine and collidine were found to intercalate $TaS_{2-x}Se_x$ for $x \leqq 1.4$, and superconducting transition temperatures were measured for both intercalated and unintercalated samples. The highest T_c obtained was 4.1 K in the $4H(c)$ phase of the sample $TaS_{1.6}Se_{0.4}$.

I. Introduction

We have been interested for some time now in the intercalation properties of many of the transition metal dichalcogenides. The $2H(a)$ phase of TaS_2, in particular, has been found to be readily intercalated by a vast range of organic compounds (*1*), but a complete investigation of the properties of the intercalated material has been handicapped by the fact that TaS_2 only forms very poor single crystals. $2H(a)$ $TaSe_2$, on the other hand, forms much more nearly perfect crystals but is not readily intercalated. It was felt that samples of the mixed anion system $TaS_{2-x}Se_x$ would be sufficiently well formed to carry out single crystal measurements, yet would also intercalate. This paper deals with the preparation and properties of this system, both intercalated and unintercalated. A preliminary report was presented at the 13th International Conference on Low Temperature Physics.

Systematic studies of the structural properties of TaS_2, $TaSe_2$, and intercalated TaS_2 have been carried out by a number of authors (*2*, *3*). The following is a brief summary of their findings. TaS_2 and $TaSe_2$ crystallize in a number of different layered polymorphs. Each layer is made up of a sandwich or slab. The smaller metal atoms in the middle fit into pockets formed by hexagonally close packed chalcogen planes. The chalcogen planes can either fit directly over each other (giving rise to an AbA sequence), or alternatively, the second chalcogen plane can fit into pockets of the first plane not occupied by the metal atoms (AbC sequence). The first type of slab gives a trigonal prismatic environment of the metal atoms, while the second type has octahedral coordination. Finally, the various polymorphs of TaS_2 and $TaSe_2$ are built up by arranging these slabs in various sequences.

Figure 1 gives the phase diagram for TaS_2 and $TaSe_2$ and also introduces the various polymorphs. It will be noticed that the low temperature phases in both compounds have purely trigonal prismatic coordination. Phases at intermediate temperature ranges are mixed octahedral and trigonal prismatic while the high temperature phases are purely octahedral. Figure 2 shows schematic representations of the various polytypes in the $(11\bar{2}0)$ plane.

Wilson and Yoffe (*4*), Thompson et al. (*5*, *6*) and Lee et al. (*7*) have measured the electrical properties of TaS_2 and $TaSe_2$ and for the most part have found corresponding phases of these two compounds to be similar. The band structure, and hence the electrical properties, of these compounds appears to be primarily determined by the coordination of the metal ions. The $2H(a)$ and $3R$ phases of TaS_2 and $TaSe_2$ have purely trigonal prismatic coordination and are metallic.

* Research supported by Office of Naval Research.

† Hertz Foundation Fellow, 1971–72.

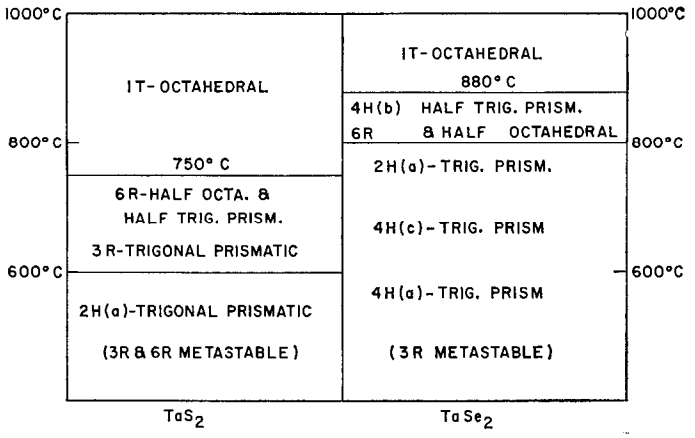

FIG. 1. Phases of TaS_2 and $TaSe_2$.

$1T$ TaS_2 and $TaSe_2$, on the other hand, possess octahedral coordination of the metal ion; the former displays "semiconducting" electrical transport properties (*5*, *8*) while the present investigation has indicated that the latter is metallic. It should be noted that the interpretation of the electrical data for the $1T$ phases is open to some question owing to the uncertain role of the impurities. The $4H(b)$ phase of TaS_2, with mixed trigonal prismatic and octahedral coordination, shows metallic conductivity along the a axis and semiconducting conductivity along the c axis (*9*).

Wilson and Yoffe's qualitative model for the band structure of transition metal dichalcogenides describes the conduction band as a linear combination of metal d-orbitals. The conduction band in octahedrally coordinated compounds is formed from the degenerate "t_{2g}" d-orbitals (d_{xy}, d_{yz}, d_{xz}), while in the trigonal prismatic coordination a lower symmetry splits the conduction band into two. The lower band is formed from the metal d_{z^2} orbital, while the upper is formed from a linear combination of the metal $d_{x^2-y^2}$ and d_{xy} orbitals. For both trigonal prismatic and octahedral Group V B dichalcogenides, excluding the ditellurides which form distorted bonds due to formation of Te–Te chains, one of the five metal valence electrons is given to the conduction band. Twelve chalcogen valence electrons and four out of five metal electrons go into bonding orbitals. Consequently, the model predicts that both the octahedral and trigonal prismatic modifications of TaS_2 and $TaSe_2$ should be metallic. Since the model completely neglects layer–layer interactions, it also predicts similar electrical behavior for phases with different stacking orders but the same metal coordination.

Organo-metallic complexes are formed by

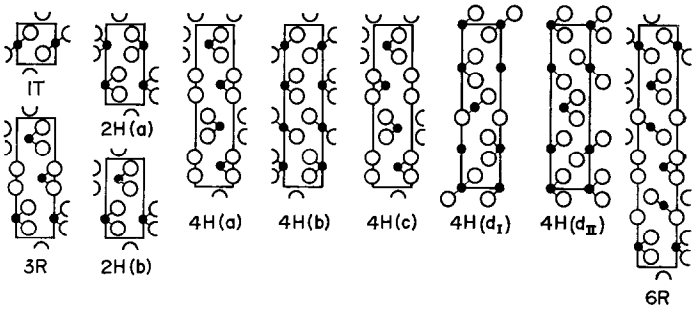

FIG. 2. Sections through the $(11\bar{2}0)$ plane of the various polymorphic forms seen in layered transition metal dichalcogenides. The small black circles represent the metal atoms and the larger open circles represent the chalcogen atoms. [see Refs. (*2* and *3*)].

TaS_2 and organic molecules such as pyridine or substituted pyridines, with the organic material penetrating the van der Waals gap between the successive S–Ta–S slabs. The plane of the aromatic ring lies parallel to the slabs (*1*). These particular organic compounds were chosen for our study in the mixed anion system because of the ease with which they intercalate, as well as their stability in TaS_2. The aliphatic amine octadecylamine ($CH_3(CH_2)_{17}NH_2$) also intercalates TaS_2 but goes in so that the chains are nearly parallel to the crystallographic c axis, the degree of alignment depending on the rate of intercalation. The c-spacing in this complex is increased by as much as 50 Å, but this expansion is seen only by intercalating slowly at room temperatures (*1*).

The ability of an organic molecule to intercalate seems to be strongly associated with its Lewis basicity. Strong Lewis bases ($pK_a > 4$) seem to form stable complexes in which electrons are donated to partially filled sulfur orbitals. X-Ray studies indicate that in many cases a high degree of horizontal registry is maintained between successive TaS_2 slabs after intercalation. This, together with geometrical considerations and the fact that these ordered complexes are stoichiometric, indicates that the "donation-bonding" must be to specific sites on the sulfur atoms. Furthermore, X-ray electron emission measurements (ESCA) indicate that the bonding is to the nitrogen atoms in the organic moelcule. Finally, it has been found that the stoichiometry for a particular organic molecule seems to be independent of the particular disulfide that it intercalates. For example, $TaS_2(pyridine)_{1/2}$, $NbS_2(pyridine)_{1/2}$, and $TiS_2(pyridine)_{1/2}$ are all observed (*1*).

The remainder of this paper is divided into five sections. In Sects. II and III sample preparation and X-ray analyses are discussed. Section IV deals with the phase diagram of unintercalated $TaS_{2-x}Se_x$ while Sect. V deals with the intercalation properties of the system. In Sect. VI we present the superconducting and electrical transport properties of the system.

II. Sample Preparation

Powder samples of the mixed anion system were prepared by heating stoichiometric mixtures of the elements in evacuated sealed quartz tubes. These samples were reacted at 950°C for 1 wk and cooled slowly over a further period of 1 wk to 300°C, where they annealed for a similar length of time. Single crystals were prepared using the vapor transport method of Schäfer (*10*), usually by prereacting the elements in the presence of iodine at 950°C for several days followed by transport from 870 to 750°C over a period of about 10 days. These samples were then annealed at 500°C for several days and cooled to room temperature in 4 or 5 hr. An alternate method for growing crystals was to allow the elements and iodine to sit in a uniform temperature of about 950°C for 10 days followed by a similar annealing procedure.

Selected samples (both crystal and powder) were reheated to 900°C and annealed there for several days. Some of these samples were quenched by pulling them out of the oven and immediately plunging them into cold water. Other samples were cooled to 700 or 500°C, reannealed at those temperatures for several days, and then quenched. Other samples were reannealed at 300°C for 3 wk and cooled slowly to room temperature.

$2H(a)$ TaS_2 forms wrinkled grey-black crystals while those of $2H(a)$ $TaSe_2$ are flat and silver. Mixed anion crystals in the $2H(a)$ or $4H(c)$ phases were generally smooth, shiny black or silver hexagons with thicknesses ranging from 25 μm to 2 mm and areas from 1 to 20 mm^2. Crystals of $1T$ TaS_2, $TaSe_2$, and $TaS_{2-x}Se_x$ were very flat, shiny gold hexagons. Pure $1T$ $TaSe_2$ could be obtained only by quenching samples from 900°C with excess selenium. In some cases the samples quenched from 500°C for $x \geqq 1.6$ contained traces of TaX_3 (where X = S or Se). The trichalcogenides took the distinctive form of silver lath-shaped needles.

Confidence in composition and homogeneity of unintercalated samples was based upon several factors. First of all, the components of each sample were weighed out to better than one part in 10^3 and no excess chalcogen was observed in the quartz tubes after reaction. X-Ray analysis shows monotonic, smoothly varying a and c/n (the crystallographic repeat distance, c, divided by n, the number of layers in the polymorph) spacings as a function of composition, indicating a continuous solubility range from $x = 0$ to $x = 2$. In those samples where two or more polytypes coexisted, the a and c/n parameters were found to correspond to polymorphs of the same composition. Chemical analyses (*11*, *12*) confirmed both the Ta and Se content to within approximately 0.5%. It was noticed, however,

that the sulfur analyses were high in most samples by 1 to 2%. It was determined that this was due to a systematic error introduced by selenium in the sulfur analysis.

Intercalated samples were prepared by sealing $TaS_{2-x}Se_x$ powder or crystals with the organic liquid in evacuated thick-walled (~1/8 in.) Pyrex ampoules. Organic materials that are solid at room temperature such as octadecylamine were either dissolved in a suitable solvent (e.g., benzene) before sealing or added to the ampoule as a solid. Pyridine samples intercalated within three days by heating to 150°C. The octadecylamine sample intercalated after four days at 90°C. [Note: Because of the elevated temperature, the full 50 Å spacing that is seen in TaS_2 intercalated with octadecylamine at room temperature was not seen (see Sect. V).] The substituted pyridine samples were heated to 200°C for about 2 or 3 wk. Stoichiometry of the intercalated samples was determined by carefully weighing the sample both before and after intercalation. The intercalated sample was rinsed thoroughly in CH_2Cl_2 and dried before weighing in order to remove any unintercalated organic material. In this fashion, percentage weight gains due to intercalation could be determined within ±2%.

III. X-Ray Analysis

Cu$K\alpha$ radiation was used with Picker diffractometer and scintillation counter to obtain X-ray data. Samples were ground with mortar and pestle to a fine powder (grain size $\leqq 53$ μm) and reground after dispersion in Canada balsam. This was done in order to reduce the effects of preferred orientation on the intensity measurement. The sensitivity of the method to secondary phases was determined by mixing various ratios of finely ground pure $1T$ and $2H$ TaS_2 powder. The relative intensities of corresponding $00l$ lines of the two phases as a function of composition of the mixture were compared. It was found that secondary phases could be detected in concentrations as low as 3%.

The a and c parameters of the samples were determined with the aid of a computer program by minimizing the rms deviation between calculated d-spacings and those observed in the diffractograms. Both the a and c axes of all phases increase monotonically with x. Figures 3 and 4 show the slab thickness, c/n, and the a axis, respectively, as a function of x for the $1T$, $2H(a)$, $3R$ and $6R$ phases. Several $4H$ phases were found and are also shown. The increase in unit cell dimension from TaS_2 to $TaSe_2$ corresponds to the increase in atomic radius from S to Se. Similar results are reported in the system $NbSe_{2-x}Te_x$ (*13*).

Typically, c/n for unintercalated samples could be measured to within ±0.003 Å (the uncertainty in determining the center of lines was about ±0.05° at $2\theta \cong 100°$) and the a axis to within ±0.002 Å. The lattice parameters for the intercalated samples, however, could only be determined to within ±0.01 Å for c/n and ±0.004 Å for a.

Although an attempt was made to analyze in detail the structure of representative compositions of intercalated as well as unintercalated samples, such an analysis was hampered by the

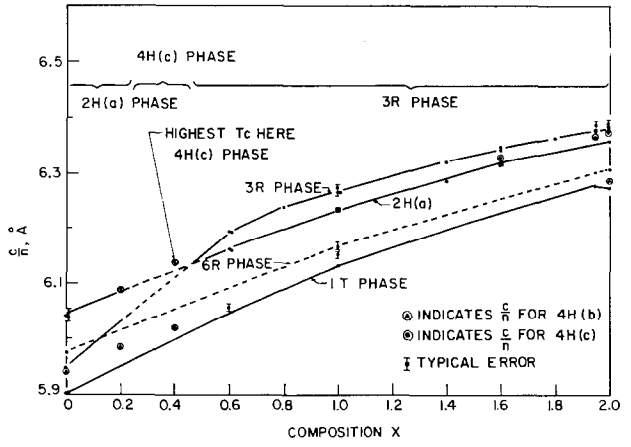

FIG. 3. Comparison of c/n vs x for various phases of $TaS_{2-x}Se_x$.

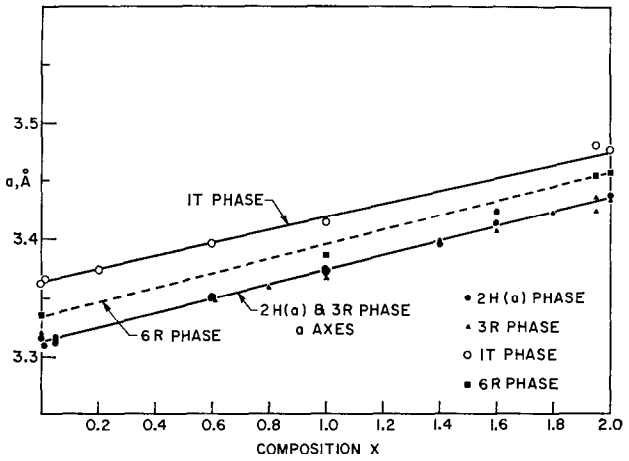

FIG. 4. a Axis vs x for various phases of $TaS_{2-x}Se_x$.

effects of preferred orientation and disorder-broadening. The patterns from intercalated samples were too disordered and the scattering from the organic molecule too weak to obtain meaningful information on the location of the various atoms in the unit cell. Only a few of the unintercalated samples could be analyzed in detail. In general, the $1T$ phases gave the sharpest

TABLE I

$2H$ $TaS_{0.4}Se_{1.6}$ INTENSITY FIT[a]

				Composite ($S_{0.2}Se_{0.8}$)		Ordered anions
$h\,k\,l$	d_{calcd}	d_{obsd}	(I/I_{max})obsd[b]	(I/I_{max}) $2H(a)_{calcd}$	(I/I_{max}) $2H(b)_{calcd}$	(I/I_{max}) $2H(a)_{calcd}$
0 0 1	12.635	—	0.00	0.000	0.000	0.02
0 0 2	6.318	6.34	1.00	1.000	1.0000	1.00
0 0 3	4.212	—	0.00	0.000	0.000	0.002
0 0 4	3.159	3.167	0.01	0.003	0.003	0.004
1 0 0	2.9570	2.9585	0.12	0.133	0.390	0.159
1 0 1	2.8792	2.8820	0.14	0.243	0.082	0.241
1 0 2	2.6782	2.6815	0.55	0.642	0.161	0.726
0 0 5	2.5270	—	0.00	0.000	0.000	0.0005
1 0 3	2.4201	2.4195	0.11	0.145	0.942	0.145
1 0 4	2.1587	2.1600	0.55	0.675	0.001	0.78
0 0 6	2.1059	2.1080	0.18	0.048	0.048	0.06
1 0 5	1.9211	1.9205	0.04	0.070	0.432	0.07
0 0 7	1.8050	—	0.00	0.000	0.000	0.0002
1 0 6	1.7153	1.7098	0.30	0.132	0.033	0.186
1 1 0	1.7072			0.255	0.255	0.306
1 1 1	1.6919	—	0.00	0.000	0.000	0.0008
1 1 2	1.6481	1.6451	0.08	0.113	0.113	0.163
1 1 3	1.5822	—	0.00	0.000	0.000	0.0007
0 0 8	1.5794	1.5806	0.13	0.063	0.063	0.079
1 0 7	1.5407	1.5404	0.03	0.033	0.005	0.034
1 1 4	1.5019	—	0.00	0.001	0.001	0.004

[a] $a = 3.414$ Å; $c = 12.635$ Å.

[b] No correction for preferred orientation.

and most distinct X-ray patterns, due presumably to the simplicity of the stacking arrangement in this particular phase. This allows the preservation of stacking order even when edge dislocations are introduced (*2*). The $2H(a)$, $3R$, and $4H$ phases showed considerable stacking disorder. This was evidenced by the fact that these phases gave sharp $00l$ lines while the $10l$ lines were weak and broad, the line width increasing with l. Furthermore, the fact that the hkl (where $h-k = 3n$) lines were very sharp indicates that the stacking disorder is not completely random; successive X–M–X slabs are still close packed (*14*).

Intensity patterns for unintercalated samples were calculated using atomic scattering factors derived from Moore's parameters for the unionized elements (*15*). Table I gives a comparison of the observed and calculated intensities for $2H$-$TaS_{0.4}Se_{1.6}$. The intensities were calculated on the assumption of a random distribution of sulfur and selenium. It is clear from a comparison of the $10l$ lines that the observed intensities correspond more closely with those calculated for the $2H(a)$ phase. The intensity was also calculated for the $2H(a)$ phase assuming that alternate slabs contained selenium, and a 40% S–60% Se mixture. Although this form of substitutional ordering should give the most marked effect on the $00l$ lines, which in turn are the easiest to detect, the calculation shows that only slight changes are to be expected. However, complete absence of any 001 reflection indicates that this form of substitutional order is not present; less extreme forms may well occur.

The $4H$ phases were in general the most difficult to analyze. In all, there are 10 possible $4H$ polytypes with purely trigonal prismatic coordination and 18 types with alternate trigonal prismatic and octahedral coordination (*16*, *17*). Intensities were calculated for all these structures, as well as for certain structures with only octahedral coordination, and were compared to the observed intensities of the $4H$ samples. The closest agreement with the observed intensities of $4H$ TaS_2 and $TaS_{1.8}Se_{0.2}$ was obtained with $4H(b)$ modification. On the other hand, the interpretation of the $4H$ patterns for samples at compositions $x = 0.4$, 1.6, and 1.95 were less certain due to stacking disorder. Systematic variations of the line intensities with x, as well as the relatively large values of c/n (see Sect. IV), led us to conclude these samples to be of the type $4H(c)$.

Least certain was the structure of the $4H$ samples at $x = 0.8$. The best intensity fits for this sample [assuming a single phase to be present] were obtained for those modifications in which three of the four Ta atoms in the unit cell are aligned along the c axis in the positions (0, 0, z) and one in the off-axis position ($\pm 1/3$, $\pm 2/3$, z). The $4H(a)$ polytype is the only one that both satisfies this description and exists in $TaSe_2$. It is quite possible, however, that two phases with identical a and c/n parameters are present; the observed pattern could be explained as the superposition of the patterns for the $4H(c)$ and $2H(a)$ phases.

IV. The Phase Diagram of $TaS_{2-x}Se_x$

A. Experimental Results

The general characteristics of the samples as a function of composition may be summarized as follows:

1. The phases generally separate into low, medium, and high temperature forms for all x. The $2H(a)$, $3R$ and $4H(c)$ (purely trigonal prismatic) phases occur in the low temperature region, the $4H(b)$ or $6R$ phases occur in an intermediate range, and the octahedral $1T$ phase occurs at highest temperatures. The temperature at which the $1T$ stabilizes seems to increase with Se content.

2. In the low temperature region for $x > 0.4$ the $3R$ phase predominates, but for $x < 0.02$ the $2H(a)$ phase is stable. Several samples in the region $x > 0.4$ were reannealed at 300°C for 3 wk and slowly cooled to room temperature. X-Rays of these samples showed the $3R$ phase to remain while the $2H(a)$ phase seemed to diminish and in some cases disappeared completely. For $0.2 < x < 0.4$ the $4H(c)$ phase exists at low temperatures, although the 2H(a) phase has been prepared as a powder.

3. The intermediate temperature region ($500°C \leqq T \leqq 900°C$) is complex. Near the TaS_2 end of the range the $6R$ and $4H(b)$ phases coexist. Our work confirms the existence of the $4H(b)$ phase in TaS_2 reported by Di Salvo et al. (*9*). Compositions in the range $0.2 \lesssim x \lesssim 0.4$ were found to be in the $4H(b)$ phase. For $x \geqq 0.8$ it appears as if the $4H(c)$ and possibly the $2H(a)$ polytypes coexist in the temperature range 500 to 700°C while the $6R$ and $4H(b)$ phases extend from 700 to 900°C. Possibly yet another phase region extends from $0.4 \lesssim x \lesssim 0.8$ in the temperature range 500 to 900°C. However, this region may be just an extension of the $x \geqq 0.8$ region as suggested at the end of Sect. III.

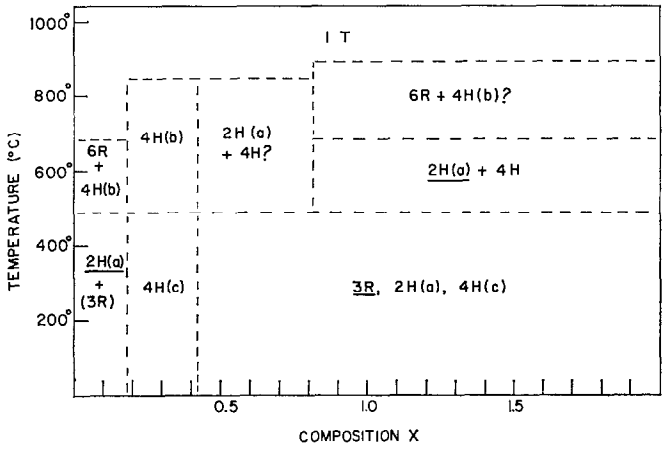

FIG. 5. Phase diagram for $TaS_{2-x}Se_x$.

4. For $x > 0.4$ a pure $1T$ phase could not be obtained by quenching. Several samples were reheated to 900°C with excess S and Se and quenched in an attempt to stabilize this phase, but it could be only stabilized (with the correct lattice parameters) in the cases of TaS_2 and $TaSe_2$. The mixed anion samples separated into two $1T$ phases, corresponding to slightly different compositions.

A phase diagram was drawn to be consistent with the above results, the observations of TaS_2 and $TaSe_2$ by other investigators, and the possibility that samples quenched from higher temperatures might convert to the lower temperature modifications. This is shown in Fig. 5.

B. Discussion of the Phase Diagram

As mentioned earlier, the $3R$ phase seems to be the most stable at room temperature for $x > 0.4$. Huisman has considered the relative stabilities of the $2H(a)$ and $3R$ phases in $TaSe_2$ (*18*). He found that $3R$ $TaSe_2$ could be obtained as a single phase by reacting the elements at a relatively low temperature (~500–600°C), or could be obtained in a mixture with the $2H(a)$ phase by cooling samples from ~1000°C at a rate greater than 10°C/hr. Nearly pure $2H(a)$ $TaSe_2$, on the other hand, was obtained either by quenching the sample from 700°C or by cooling at a very slow rate (10°C/hr or less). Huisman concluded that the $3R$ phase was metastable at all temperatures and that its formation was due to kinematic reasons; higher temperature phases such as $1T$ or $6R$ could convert more readily to the $3R$ phase than to the $2H(a)$ phases. There is agreement between Huisman's work and the present investigation for samples quenched from above 500°C or cooled from 1000°C at a moderate rate. However, it is not clear that Huisman's conclusion about the relative stabilities of the $3R$ and $2H(a)$ phases is entirely correct. Although we have observed that the $2H(a)$ phase can be obtained by quenching from 500°C those samples with $x \gtrsim 0.4$, annealing them at 300°C before quenching generally resulted in the formation of the $3R$ phase. Chemical analysis showed that no changes in composition occurred during quenching and annealing.

An interesting correlation can be made between the stability of the phase and its slab thickness, c/n. From Fig. 3 it will be noticed that somewhere near the composition $x = 0.4$ the slab thickness for the $2H(a)$ and $3R$ phases are the same. For $x < 0.4$, the $2H(a)$ phase has the larger slab thickness while for $x > 0.4$, the $3R$ phase has a larger c/n. When viewed in light of the phase diagram (Fig. 5), it is seen that this crossover occurs precisely in the composition range where the predominant low temperature phase changes from $2H(a)$ to $3R$. The larger slab thickness is apparently associated with the most stable phase. It is interesting to note that in general, the smaller the slab thickness of a phase, the higher the temperature at which that phase becomes stable. A comparison of Figs. 3 and 4 shows that the volume of the unit cell is almost independent of the polytype.

Another observation to be made in connection with the phase diagram is that the phases with more octahedral character occur at higher

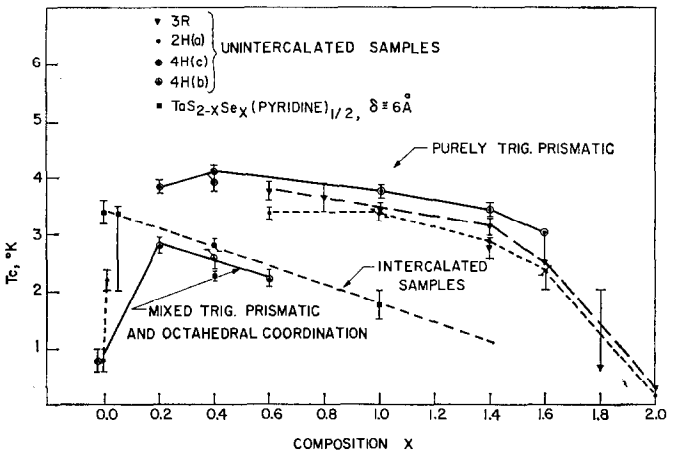

FIG. 6. T_c vs x in $TaS_{2-x}Se_x$ and $TaS_{2-x}Se_x$ (pyridine)$_{1/2}$.

temperatures. It has been shown from molecular orbital calculations (*18*, *19*) that covalency of the metal in the VB and VIB dichalcogenides is responsible for the lower internal energy of the trigonal prismatic metal coordination as compared to octahedral coordination. Thus, the $2H(a)$ and $3R$ phases tend to be found at low temperature, where internal energy considerations determine the structure. At much higher temperatures, on the other hand, contributions to the entropy from the optical branches of the phonon spectrum become significant. Accurate measurements of the anisotropic Debye-Waller factor in β-ThI_2, which has a layer structure isomorphic with the $4H(b)$ polytype (mixed octahedral and trigonal prismatic), indicate that optical modes polarized normal to the c axis of the octahedrally coordinated metal ions may be softer than those of the trigonal prismatic ions (*20*). This fact might indicate, then, that phases with more octahedral coordination have greater entropy. Indeed, differential thermal analysis made by Huisman (*18*) on $TaSe_2$ shows an increase in entropy with increasing octahedral character. Thus, as Huisman has pointed out, the octahedral phase becomes stable at high temperatures when the entropy term in the Gibbs free energy becomes dominant.

V. Intercalation

Intercalated $TaS_{2-x}Se_x$ samples were found to be quite similar to the TaS_2 intercalates prepared by Gamble et al. (*1*). For $x \geqq 1.6$ no intercalation was observed, while those samples with $x < 1.6$ usually formed stable complexes of the type $TaS_{2-x}Se_x$(organic)$_{m/n}$, where m and n are integers. We have observed that for pyridine intercalates $m/n \cong 1/2$, for collidine $m/n \cong 1/6$, and for 4-picoline $m/n \cong 1/3$. Octadecylamine, a long chain amine has $m/n \cong 2/3$. Table II gives X-ray results for the pyridine and collidine intercalated samples. Note that the pyridine samples at $x = 0.4$ retains its 4-layer structure after intercalation. In octadecylamine samples the increase, δ, in the layer spacing was about 29 Å. In all cases, the a axis showed a very slight increase (<1 %) upon intercalation.

The organic molecules apparently go in the van der Waals region between successive X–M–X slabs. Again, as in TaS_2, we can explain the observed lattice spacings by assuming two pyridine rings (each of which is ~3 Å thick and ~6 Å long) go between successive X–M–X slabs so that the planes of the rings are normal to the c axis. Note it is also possible that the pyridine goes in as a single layer on end rather than as a bilayer. Two other minority phases were observed for the $x = 1.0$, $y = 0.47$ pyridine sample. Evidently the intercalation reaction did not proceed to completion ($y = 0.47$ rather than 0.50). The minority phases reflect this incomplete intercalation and correspond most simply to pyridines intercalating every second X–M–X slab only, and in the case of the phase with $c/n = 15.8$ Å, apparently only one pyridine ring lies between every other layer. Other samples of this "stagewise" intercalation are seen in both pyridine and collidine samples at $x = 1.4$. Notice also that only one layer of collidine molecules

TABLE II

LATTICE PARAMETERS OF $TaS_{2-x}Se_x$(PYRIDINE)$_y$ AND $TaS_{2-x}Se_x$(COLLIDINE)$_y$ (Å)[a]

		Pyridine				Collidine			
x	Phase before interc.	y	c-Spacing before interc.	c-Spacing after interc.	δ	y	c-Spacing before interc.	c-Spacing after interc.	δ
0	$2H(a)$	0.496	2×6.038	2×12.03	5.99	0.165	2×6.04	2×9.67	3.63
0.05	$2H(a)$	0.47	2×6.05	2×12.03	5.98				
0.4	$4H(c)$	0.48	4×6.14	4×12.07	5.93				
0.6	$3R$					0.12	3×6.19	2×9.86	3.67
1.0	$2H(a)$	0.47	2×6.25	2×12.24	5.99				
		?	2×6.25	2×18.42	5.92				
		?	2×6.24	$(?)\times 15.8$	3.3				
1.4	$2H(a)$	?	2×6.29	$(?)\times 12.25$	5.96				
			2×6.29	$(?)\times 18.64$	6.06				
	$3R$					?	3×6.32	2×10.02	3.70
							3×6.32	$(?)\times 16.43$	3.78

[a] Every other layer is intercalated; $18.42 = 2\times 6.25 + 5.92$. The unit cell is composed of two of these 18.42 Å slabs stacked on the other.

goes between metal layers ($\delta \cong 3.7$ Å), compared to the bilayer of most pyridine samples.

VI. Superconductivity and Electrical Properties

Figure 6 shows the superconducting transition temperatures plotted against x for both unintercalated and pyridine-intercalated samples. The transitions were determined by measurements of ac susceptibility. We observe a very sharp rise in T_c as very small amounts of selenium are substituted for sulfur in TaS_2. T_c increases from 0.8 K for $2H(a)$ TaS_2 to a maximum of 4.1 K in the vicinity of $x = 0.4$ [$4H(c)$ phase]. Note that there is little difference between the T_c values measured for the purely trigonal prismatic samples $2H(a)$, $4H(c)$, and $3R$ for any given composition. This is to be contrasted with the lower transition temperature of the mixed-coordination $4H(b)$ samples. No superconducting transitions have been observed in the $1T$ (octahedral) phases down to 1.4 K. For $x > 1.4$ T_c begins to drop rapidly, eventually assuming the values 0.15 and 0.22 K for the $2H(a)$ and $3R$ $TaSe_2$ (*4*).

The intercalated samples showed a gradual drop in T_c from TaS_2 to $TaS_{1.0}Se_{1.0}$. In all cases, except for $x \leqq 0.05$, the transition temperature drops upon intercalation, and in most cases, the width of the transition increases. A notable exception is $TaS_{1.6}Se_{0.4}(pyr)_{1/2}$, which remains quite sharp. In this material T_c is 2.8 K for the $4H(b)$ phase but is 2.4 K in the $4H(c)$ phase.

a Axis resistivities of various unintercalated (purely trigonal prismatic) crystals were measured from 4 to 400 K using a 4-point probe. Absolute values at room temperature were measured using the van der Pauws technique, but uncertainties in the thickness determination lead to errors of $\pm 10\%$. The resistivity (in the mixed system) is similar to that of TaS_2 and $TaSe_2$.

Figure 7 shows $\rho(T)$ for several compositions. Note that a change of slope occurs in $TaSe_2$ at ~110 K. This "kink" is also seen in $2H(a)$ TaS_2 at 70 K, as well as in mixed anion samples, and is presumably related to a slight lattice distortion (*21*). In the mixed anion samples, however, it is much less pronounced. We note that the temperature-dependent term in the resistivity of the sample $TaS_{1.6}Se_{0.4}$ is much greater than any of the other compositions, although only one sample was measured. This particular sample also showed the highest superconducting transition temperature, indicating that an enhanced phonon–electron interaction may be responsible for the higher T_c. The residual resistance at 4.2 K increases slightly at the center of the composition range, due, no doubt, to increased impurity scattering.

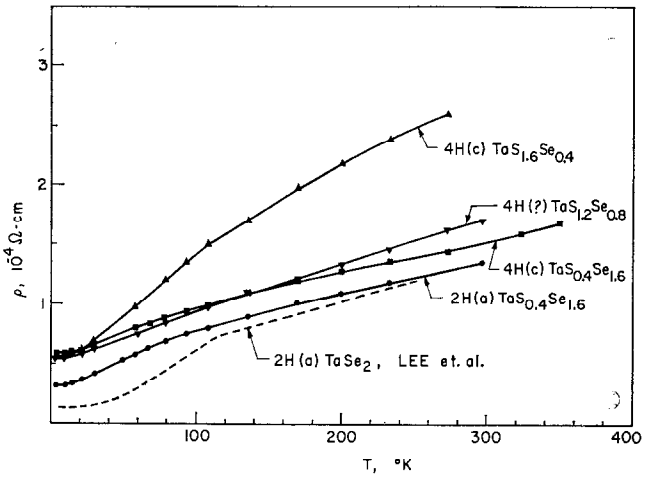

FIG. 7. *a* Axis resistivity vs temperature for trigonal prismatic $TaS_{2-x}Se_x$.

The Hall coefficient, R_H, was measured as a function of composition at room temperature and was positive in all cases. The density of holes, calculated assuming single band conduction, is roughly twice the density of Ta atoms. In addition, the signs of the Hall and Seebeck coefficients were opposite, although we did not make accurate measurements of the Seebeck coefficient. These same phenomena have been seen in 2*H* TaS_2 and have been attributed to the fact that conduction takes place via two overlapping bands rather than a single *d* band (*6*).

Summary

Large, well-formed crystals of the mixed anion system $TaS_{2-x}Se_x$ have been shown to exhibit intercalation properties similar to TaS_2 for $x < 1.6$. From empirical observation of color, electrical resistivity, and superconducting transition temperature, we conclude that the physical properties of the system are principally determined by the coordination of the Ta atoms. Those phases with pure trigonal prismatic character have higher T_c values, are electrically metallic, and usually are stable at low temperatures. As we go to phases with half octahedral and half trigonal prismatic character, we observe lower T_c values and less metallic character. In the limit of pure octahedral coordination, we observe no superconducting transition temperature and semiconducting behavior (at least for 1*T* TaS_2). The observations are in agreement with those of other investigators (*3*, *22*). A rigid band model would seem to be appropriate for the 2*H* phase of the system $TaS_{2-x}Se_x$ in view of the similarity of the electrical and structural properties observed throughout the entire composition range. Indeed, a rigid band is reasonable in light of the model proposed by Wilson and Yoffe (*4*), who maintain that the chalcogen orbitals are concerned mainly with bonding and have little influence on the conduction band.

In conclusion, we have shown that crystals of $TaS_{2-x}Se_x$ with $0.4 < x < 1.6$ and with trigonal prismatic coordination of the Ta are well formed and may be readily intercalated. These crystals should prove valuable in further studies of the intercalated layered transition metal dichalcogenides.

Acknowledgments

We thank Professor T. H. Geballe for helpful discussions during the course of this work.

References

1. F. R. GAMBLE, F. J. DI SALVO, R. A. KLEMM, AND T. H. GEBALLE, *Science* **168**, 568 (1970).
2. F. JELLINEK, *J. Less-Common Metals* **4**, 9 (1962).
3. R. HUISMAN AND F. JELLINEK, *J. Less-Common Metals* **17**, 111 (1969).
4. J. A. WILSON AND A. D. YOFFE, *Advan. Phys.* **18**, 193 (1969).
5. A. H. THOMPSON, F. R. GAMBLE, AND J. F. REVELLI, *Solid State Commun.* **9**, 981 (1971).

6. A. H. THOMPSON, F. R. GAMBLE, AND R. F. KOEHLER, *Phys. Rev. B* **5**, 2811 (1972).
7. H. N. S. LEE, M. GARCIA, H. MCKINZIE, AND A. WOLD, *J. Solid State Chem.* **1**, 190 (1970).
8. J. A. BENDA, C. N. KING, K. R. PISHARODY, AND W. A. PHILLIPS, *Proc. Int. Conf. Low Temperature Phys. LT-13, 13th*, Boulder, CO, Aug. *1972*, in press.
9. F. J. DI SALVO, B. G. BAGLEY, J. M. VOORHOEVE, AND J. V. WASZCZAK, unpublished data.
10. H. SCHÄFER, "Chemical Transport Reactions." Academic Press, New York (1964).
11. E. MEIER AND N. SHALTIEL, *Mikrochim. Acta* **4**, 580 (1960).
12. G. INGRAM, "Methods of Organic Elemental Microanalysis." Reinhold, New York (1962).
13. E. A. ANTONOVA, K. V. KISELEVA, AND S. A. MEDVEDEV, *J. Exp. Theor. Phys.* **32**, 31 (1971).
14. A. GUINIER, "X-Ray Diffraction in Crystals, Imperfect Crystals, and Amorphous Bodies," Chap. 7 Freeman, San Francisco (1963).
15. F. H. MOORE, *Acta Crystallogr.* **16**, 1169 (1963).
16. B. E. BROWN AND D. J. BEERNTSEN, *Acta Crystallogr.* **18**, 31 (1965).
17. F. KADIJK AND F. JELLINEK, *J. Less-Common Metals* **23**, 437 (1971).
18. R. HUISMAN, PhD dissertation, Univ. of Groningen, 1970 (unpublished).
19. R. HUISMAN, R. DE JONGE, C. HAAS, AND F. JELLINEK, *J. Solid State Chem.* **3**, 56 (1971).
20. L. J. GUGGENBERGER AND R. A. JACBOSON, *Inorg. Chem.* **7**, 2257 (1968).
21. E. EHRENFREUND, A. C. GOSSARD, F. R. GAMBLE, AND T. H. GEBALLE, *J. Appl. Phys.* **42**, 1491 (1971).
22. W. GEERSTMA, C. HAAS, R. HUISMAN, AND F. JELLINEK, *Solid State Commun.* **10**, 75 (1972).